Plant Science 263 (2017) 1–11

Contents lists available at ScienceDirect

Plant Science

journal homepage: www.elsevier.com/locate/plantsci

Involvement of *SchRabGDI1* from *Solanum chilense* in endocytic trafficking and tolerance to salt stress

Alex San Martín-Davison[a], Ricardo Pérez-Díaz[a], Flavia Soto[a], José Madrid-Espinoza[a], Enrique González-Villanueva[a], Lorena Pizarro[b], Lorena Norambuena[b], Jaime Tapia[c], Hiromi Tajima[d], Eduardo Blumwald[d], Simón Ruiz-Lara[a,*]

[a] *Instituto de Ciencias Biológicas, Universidad de Talca, 2 Norte 685, Talca, Chile*
[b] *Centro de Biología Molecular Vegetal, Facultad de Ciencias, Universidad de Chile, Santiago, Chile*
[c] *Instituto de Química de los Recursos Naturales, Universidad de Talca, 2 Norte 685, Talca, Chile*
[d] *Department of Plant Sciences, University of California, Davis, CA 95616, USA*

ARTICLE INFO

Keywords:
GDP dissociation inhibitors
RabGTPases
Vesicular trafficking
Salt stress
Endocytic pathways
Solanum

ABSTRACT

Physiological responses of plants to salinity stress requires the coordinated activation of many genes. A salt-induced gene was isolated from roots of the wild tomato species *Solanum chilense* and named *SchRabGDI1* because it encodes a protein with high identity to GDP dissociation inhibitors of plants. These proteins are regulators of the RabGTPase cycle that play key roles in intracellular vesicular trafficking. The expression pattern of *SchRabGDI1* showed an early up–regulation in roots and leaves under salt stress. Functional activity of SchRabGDI1 was shown by restoring the defective phenotype of the yeast *sec19-1* mutant and the capacity of SchRabGDI1 to interact with RabGTPase was demonstrated through BiFC assays. Expression of *SchRabGDI*1 in *Arabidopsis thaliana* plants resulted in increased salt tolerance. Also, the root cells of transgenic plants showed higher rate of endocytosis under normal growth conditions and higher accumulation of sodium in vacuoles and small vesicular structures under salt stress than wild type. Our results suggest that in salt tolerant species such as *S. chilense*, bulk endocytosis is one of the early mechanisms to avoid salt stress, which requires the concerted expression of regulatory genes involved in vesicular trafficking of the endocytic pathway.

1. Introduction

Membrane trafficking in eukaryotes depends on the accurate targeting of transport vesicles to and from defined membrane-bound compartments whereby different proteins participate in distinct steps of the process. Among the proteins involved in this vesicular trafficking is the Rab/Ypt family (RabGTPases), which form the largest branch of the Ras superfamily of the small GTPases that exist in all eukaryotic cells [1]. Different members of the RabGTPase family localized in the cytoplasmic side of organelles have been shown to have specific roles in targeting and/or tethering transport vesicles during exocytosis and endocytosis in eukaryotic cells [1,2]. RabGTPases function depends on their interaction with accessory proteins and their capacity to bind and hydrolyze GTP, which translates in the alternation between “active” and “inactive” states. RabGTPases carrying a geranylgeranyl group require guanine nucleotide exchange factors (GEFs) that facilitate GDP dissociation, GTPase activating proteins (GAP) that stimulate GTP hydrolysis, and guanine dissociation inhibitors (GDI) that form soluble complexes with small GTPases by shielding their lipid group. GDI proteins play a critical role in regulating the recycling of RabGTPases, allowing their rapid recycling [3] and maintaining a cytosolic pool of available RabGTPases to be delivered to vesicle membranes [4].

Although specific GDIs for Rab GTPases (RabGDIs) have been well characterized in yeast and animals, in plants, only few genes that share homology with members of the GDI family have been reported. Whereas 57 RabGTPases members have been identified in the *Arabidopsis thaliana* genome [5], only three *RabGDI* homologues have been identified, *AtRabGDI1*, *AtRabGDI2* and *AtRabGDI3* [6–8]. Two cDNAs encoding RabGDI have been isolated from rice, *OsGDI1* and *OsGDI2* [9], one *GDI* has been cloned from tobacco [10] and chickpea [11], and three *RabGDIs* have been identified in grapevine [12]. Among all characterized RabGDI family members, five structurally and functionally sequence-conserve regions (SCRs) have been identified [4]. Mutations of residues within SCRs interrupt the binding of RabGDIs to RabGTPase proteins and may lead to a decreased RabGTPase recycling [13,14]. The ability of RabGDI to interact with distinct RabGTPases has

* Corresponding author.
E-mail address: sruiz@utalca.cl (S. Ruiz-Lara).

http://dx.doi.org/10.1016/j.plantsci.2017.06.007
Received 10 March 2017; Received in revised form 7 June 2017; Accepted 17 June 2017
Available online 28 June 2017

been demonstrated, however different RabGTPase members present distinct binding affinity [15].

Plants display different mechanisms to tolerate salt stress including ion extrusion from the cell and ion sequestration in the vacuole to prevent excess accumulation in the cytosol [16,17]. The buildup of sodium into the vacuole is mediated by the action of Na^+/H^+ antiporters located in the tonoplast [18,19]. In addition, a rapid increase in the root vacuolar volume leading to increased vacuolar salt content has been shown under salt stress [20]. During this process, endosomes are fused to the main vacuole, suggesting that vesicle trafficking might play an important role in the response to salt stress [21]. Overexpression of the *AtRabG3e* gene (encodes a RabGTPase) in *Arabidopsis* triggered accelerated endocytosis in roots, leaves, and protoplasts and resulted in accumulation of sodium in vacuoles and increased tolerance to salt and osmotic stresses [22]. Similar results have been observed with the overexpression of an *AtRabG3e* homologous gene, *PgRab7* from *Pennisetum glaucum* in tobacco [23]. Loss of function of RabA1 members involved in vesicle transport between the trans-Golgi network and the plasma membrane caused hypersensitivity to salt stress, most likely due to the participation of these proteins in the localization of cell-surface proteins, such as ion channels and pumps [24]. The involvement of RabGTPases in the response to salinity stress suggests that other interactive members controlling their function could also play a role in this response. Whereas one study has implicated an Arabidopsis RabGEF in mediating an endocytic pathway affecting stress tolerance [25], the role of RabGDIs in plant tolerance to salt stress has not been yet reported.

Cultivated species of the Solanaceae family are susceptible to a wide range of environmental stresses. For example, salinity is known to negatively affect seed germination, inhibit growth and decrease fruit productivity [26]. The Solanum section Lycopersicum includes *S. chilense*, a wild tomato species with a notable capacity to withstand salinity and drought [27]. When subjected to salt stress conditions, *S. chilense* activates the expression of a set of genes that may be associated with its capacity to adapt to its natural habitat [28–30]. Among the genes that are differentially expressed in salt treated *S. chilense* roots, we identified one encoding a protein with high homology to AtRABGDI1, hence named *SchRABGDI1*. Here, we analyzed the molecular function of SchRabGDI1 and its ability to bind RabGTPases *in vivo*. Expression of *SchRabGDI1* in *Arabidopsis thaliana* resulted enhanced tolerance to salt stress and in an increase of both the endocytosis rate in root cells and vacuolar Na^+ content upon high salt exposure. Our results suggest that salt-induced expression of *SchRabGDI1* contributes to endocytic trafficking in *S. chilense* and to its natural salt tolerance.

2. Material and methods

2.1. Plant materials and growth conditions

Solanum chilense (Dunal) seeds were obtained from plants collected in Northern Chile at a 2500 m.s.n.m. 18° 26′ lat. S 69° 45′ long. Plants were clonally propagated in pots containing a mixture of perlite, vermiculite and peat moss (1:1:1 v/v) and grown under greenhouse conditions at 23–25 °C and a 16 h/8 h light/dark photoperiod. Plants were fertilized with commercial Hoagland's solution (1/4 strength) every 10 days. For gene expression analyses under non-stressed conditions organ samples including root (R), young and mature leaves (YL, ML), stem (S), flower bud (FB) and flower (F) were taken at flowering time. Salt stress in *S. chilense* was applied to 7-week-old plants grown in 2 l pots containing a mixture of perlite:vermiculite (1:1 v/v) and fertilized with Hoaglands solution by irrigating once with 400 ml of 300 mM NaCl. Leaves and roots samples were collected at 0, 3, 6, 12, 24, 48 and 72 h after salt treatment and immediately frozen in liquid nitrogen and stored at −80 °C.

Wild-type (Col-0) and transgenic *Arabidopsis thaliana* plants were grown in a chamber at 21 °C and a 16 h light/8 h dark photoperiod. For saline stress, 5-days-old Arabidopsis seedlings grown in solid half-strength MS (Murashige and Skoog, basal salt mixture) were transferred to half-strength MS medium containing 0 or 75 mM NaCl and maintained for 15 days. Then, biomass production (fresh weight) and leaf oxidative damage were evaluated. To assess germination rate under saline stress, seeds were surface sterilized with a 2% sodium hypochlorite solution. One-hundred seeds from wild-type and transgenic lines were sown in half-strength MS plates containing 0, 50 or 75 mM NaCl and kept at 4 °C in darkness for 3 days for seed stratification. Radicle emergence was examined every 24 h during 96 h. All treatments were done in three independent experiments.

2.2. RNA isolation

Total RNA was extracted from different organs of *S. chilense* and Arabidopsis leaves using the SV Total RNA Isolation System kit (Promega). All RNA extractions for gene expression assay were done in triplicate for each organ and condition. RNA integrity was visualized by 2% agarose gel electrophoresis and RNA concentration and purity (OD_{260}/OD_{280} ratio > 1.95) were determined with a NanoDrop ND-1000 spectrophotometer (NanoDrop Technologies). RNA samples were treated with RNase free DNase I (Ambion) to remove contaminant DNA traces.

2.3. Subtractive library construction

The Clontech PCR-Select cDNA Subtraction kit was used for the preparation of a subtractive cDNA library to identify differentially expressed genes in roots of *S. chilense* under salt stress (half-strength MS supplemented with 400 mM NaCl) in hydroponic cultivation. Double-stranded cDNA synthesis was carried out on total mRNA derived from roots of stressed (tester) and normal (driver) plants. The tester and driver cDNAs were then digested with RsaI yielding blunt end fragments of approximately 400 bp length on average and processed following the manufacturer's instructions with some modifications. The tester cDNA was aliquoted into two halves, and each half was ligated with different cDNA adaptors. Adapter ligation was followed by two rounds of hybridization with an excess of driver cDNA as per manufacturer's protocol. The resultant products were subjected to two cycles of PCR with adaptor targeting primers to amplify the differentially expressed sequences. Amplifications were performed on a Stratagene Mx3000P (Agilent Technologies). First PCR master mix contained 10x PCR reaction buffer, 0.2 mM dNTPs, 0.4 μM PCR primer 1 and Advantage cDNA polymerase (Clontech). PCR was performed under the following conditions: 94 °C (25 s) followed by 30 cycles each consisting of a denaturation step at 94 °C (10 s), an annealing step at 66 °C (30 s) and an elongation step at 72 °C (1.5 min). Before using the primary PCR products as templates for secondary PCR, these were diluted 10-fold with sterile water. The second PCR master mix contained 10x PCR reaction buffer, 0.2 mM dNTPs, 0.4 μM nested PCR primer 1, 0.4 μM nested PCR primer 2 and Advantage cDNA polymerase. PCR was run through 20 cycles each consisting of 94 °C for 15 s, 66° for 30 s and 72 °C for 1.5 min. cDNA molecules were cloned non-directionally into the pGEM-T-Easy Vector (Promega). The ligation products were used to transform the *E. coli* DH5α strain *via* electroporation. Positive clones were collected and used for plasmid isolation and sequencing.

2.4. Analysis of gene expression

Gene transcript levels were analyzed by quantitative PCR (qRT-PCR) using a Stratagene Mx3000P (Agilent Technologies) system and the Brilliant SYBR Green Master Mix (Stratagene). To prepare first-strand cDNA, 2 μg of total RNA were reverse transcribed in a 20 μl reaction using the oligo d(T) and AffinityScript QPCR cDNA Synthesis Kit (Stratagene) following manufacturer's instructions. For each sample (three biological replicates), qPCR was carried out in triplicate

(technical repeats) using 10 µl Master Mix, 0.5 µl of 250 nM primers, 1 µl of diluted cDNA and nuclease-free water to a final volume of 20 µl. Amplification was followed by a melting curve analysis with continuous fluorescence acquisition during the 55–95 °C melt. The $2^{-\Delta\Delta Ct}$ method was applied to calculate the fold change of gene transcript levels [30]. The tomato transcripts were normalized against tomato *Ubiquitin3* (accession X58253) and *GAPDH* (accession U97257) genes [29,32] and Arabidopsis transcripts were normalized against *AtFbox* (accession AT5G15710) [33]. The primers used for qPCR analysis are shown in supplementary Table S1. All qPCR products obtained from *S. chilense* were previously sequenced in order to corroborate primer specificity and gene identity.

2.5. Yeast complementation assay

For yeast complementation experiments using *SchRabGDI1*, the *sec19-1* yeast mutant strain was employed. The *Saccharomyces cerevisiae* strains RSY274 (*sec19-1*) and its parental wild-type strain RSY249 were provided by R. Schekman (University of California, Berkeley, CA). The cDNA of *SchRabGDI1* was PCR-amplified (primers described in Table S2) and cloned into the entry vector pENTR™/SD/D-TOPO® (Invitrogen) to generate *pENTR-SchRabGDI1* and verified by sequencing. *pENTR-SchRabGDI1* was recombined by LR Clonase® reaction (Invitrogen) into the destination vector pYES-dest52, under control the GAL1 promoter. The resulting construct pYES-dest52-*SchRabGDI1* and the empty vector pYES-dest52 were transformed into the *sec19* mutant, whereas the wild-type strain was transformed with the empty vector. Yeast transformation was performed using the *S. cerevisiae* EasyComp™ Transformation kit (Thermo Fisher Scientific) and selection was done on Synthetic complete (SC) medium lacking uracil and supplemented with glucose to repress the *GAL1* promoter. To evaluate the *sec19* mutant phenotype and complementation capacity of *SchRabGDI1,* transformed yeast cells were grown in SC medium supplemented with galactose at 28 °C or 37 °C for 3 days.

2.6. Genetic construct and plant transformation

The coding sequence of *SchRabGD1* was amplified by PCR using the Platinum® Taq DNA Polymerase (Invitrogen) and cloned into pGEM-T vector (Promega) and sequenced (primers listed in Table S2). The PCR product was inserted into the *Xba*I-*Sac*I sites of the pBI121 binary vector to replace the β-glucuronidase (GUS) gene, resulting in the *SchRabGDI1* gene being under the control of the CaMV 35S promoter. The final expression vector was introduced into *Agrobacterium tumefaciens* strain GV3101. Transformation of *A. thaliana* Col-0 was performed using floral-dip method as described by Clough and Bent [34]. Transgenic plants were selected on half-strength MS medium containing 50 mg l^{-1} kanamycin and 500 mg l^{-1} augmentin. The kanamycin-resistant seedlings were then transferred to a substrate mixture and grown as indicated above until seed collection. The presence of the transgene was confirmed by PCR from gDNA using specific primers for the *SchRabGDI1* gene (Table S2). Isolation of genomic DNA from true leaves was performed using the WizardR Genomic DNA Purification Kit (Promega). Homozygous T3 Arabidopsis lines were selected according to their *SchRabGDI1* expression level.

2.7. Structure prediction by homology modeling

The structural models of SchRabGDI1 and SchRabG3e proteins were built by homology modeling based on crystal structures of homologous proteins. SWISS-MODEL [35] was used to select 3D models crystallized with the closest sequence homology and also to construct comparative model structures. The crystalline structure of a GDI from *Saccharomyces cerevisiae* (PDB code 1UKV; [36]) and Ypt7, a Rab7 class from *S. cerevisiae* (PDB code 4PHH; [37]) were selected based in the best homology to SchRabGDI1 and SchRabG3e, respectively. The best models for both proteins obtained by SWISS-MODEL were improved by molecular dynamic simulation and equilibration methods using Nano Molecular Dynamics (NAMDv.2.10; [38]), the Chemistry of Harvard Molecular Modeling (CHARMM27) force field [39] and the TIP3P model for water [40]. A short initial minimization of 15,000 steps was used to remove wrong contacts and for energy optimization. The molecular dynamics were done using the following conditions: 12 ns of molecular dynamics, a periodic bordering condition box (80 Å, 100 Å, 80 Å), 150 mM NaCl and 300 °K with default parameters [38]. The final 3D model of each structure was checked for its stereochemical quality and atomic coordinates with a Ramachandran map using PROCHECK [41].

2.8. Protein-protein docking

Protein-protein docking between SchRabGDI1 and SchRabG3e with CLUSPRO software [42] and structural alignment with 1UKV Rab-GDI tridimensional model of *S. cerevisiae* were used to determinate the binding platform. Then, a molecular dynamic of 12 ns with NAMD was made to evaluate the interaction among amino acids of the binding platform and determinate the free end of both proteins. This information was used to predict the location of the SCYCE and VYNE fluorescent proteins. The Python Molecular Viewer 1.4.5 [43] and the visual molecular dynamics (VMD; [44]) softwares were used for final visualizations.

2.9. In vivo interaction of SchRabGDI1 and SchRabG3e by BiFC

Full-length cDNA encoding SchRabGDI lacking the stop codon and SchRabG3e were amplified and cloned into the entry vector pDONR207 (Invitrogen, USA) to generate pENTR-GDI1 and pENTR-RabG3e, respectively (primers shown in Table S2). pENTR-GDI1 was recombined into pDEST-GWVYNE [45], generating GDI-VYNE and pENTR-SchRabG3e into pDEST-SCYCE(R)GW [45] to generate SCYCE-SchRabG3e. The NHX5 construct used in validation experiments of the specific interaction of Rab with GDI was obtained used the same entry vector as Bassil et al. [46]. The resulting constructs were transformed into Agrobacterium strain GV3101 and transformed bacteria were infiltrated into four-week-old leaves of tobacco (*Nicotiana benthamiana*). Infiltrated plants were grown in a growth chamber for 3 days at 23 °C with 16 h/8 h light/dark photoperiod. Fluorescence was evaluated in the abaxial face of infiltrated leaves and images were acquired using Zeiss LSM 710 confocal microscope. Green fluorescence signal (500–550 nm) and mRFP (585–620 nm) were collected following excitation with 488- and 561-nm lasers as described before [47].

2.10. Endocytosis of FM4-64 and sodium green staining

Plasma membrane internalization was evaluated with the endocytic tracer FM4-64 (Thermo Fisher Scientific #T-13320) in root cells of seven-day-old wild-type and transgenic Arabidopsis seedlings grown in solid MS (half-strength). For each genotype, 4 seedlings were analyzed. Seedlings were treated with 4 µM FM4-64 in half-strength liquid MS for 10 min at 4 °C. and then washed and incubated in half-strength liquid MS at 25 °C for 5 and 30 min to allow FM4-64 internalization. Images of root cells from the transition zone were captured with a LSM 710 Zeiss confocal microscope. FM4-64 was excited using a 543 nm laser and the fluorescence collected in the range of 560–650 nm. Image analyses and fluorescence quantification were performed using the FIJI-Image J software [48]. The rate of FM4-64 internalization was calculated by the ratio between the mean of the intracellular fluorescence and the mean of the whole cell fluorescence (including the plasma membrane) from 20 to 50 cells. Three biological replicates were performed.

To monitor the intracellular localization of Na^+ in root cells of wild-type and *SchRabGDI1*-expressing Arabidopsis lines, 7-day-old seedlings grown in half-strength MS plates were incubated in liquid half-strength MS supplemented with 100 mM NaCl and 4 µM FM4-64 for 12 h [21].

After treatment, seedlings were incubated with 5 μM of the sodium tracer Sodium Green™ tetraacetate (ThermoFisher Scientific #S-6901) for 30 min. The Na^+-dependent fluorescence of Sodium Green and the FM4-64 fluorescence from cells of the transition zone of the primary root were visualized under a confocal microscope. Confocal images were captured with a LSCM 710 Zeiss confocal microscope using a predetermined setting for FM4-64 and Sodium Green fluorescence obtained from the software ZEN 2012 edition. Three biological replicates were performed.

2.11. NBT staining

For the histochemical detection of superoxide radical (O^{2-}) in Arabidopsis plants subjected to salt stress (described above), the nitroblue tetrazolium (NBT) method was employed [49]. After 15 d of growth in the presence of 75 mM NaCl, plants were immersed in a solution of NBT (0.5 mg/ml dissolved in sodium phosphate buffer pH 8.0) and incubated in the dark for 12 h. Chlorophyll was removed immersing the plants in an ethanol:acetic acid:glycerol (3:1:1) solution and then heating at 90 °C for 15 min to complete discoloration.

2.12. Chemical analysis

Arabidopsis Col-0 seedlings and *35S:SchRabGDI1* lines were grown in MS (half-strength) media for seven days and then transferred to MS (half-strength) supplemented with 75 mM NaCl for 15 days. The seedlings were collected and roots and leaves were separated to quantify sodium content. The leaves and root samples were washed with bi-distilled water and dried up in a heater at 70 °C. For digestion, 0.5 g of sample was weighed out and 5 ml of Suprapur nitric acid was added. The samples were then dried almost completely under an extractor fan, with constant stirring, using a heating plate set to 90 °C. Finally, the solutions were filtered using 0.45 μm filters. The filtering process was performed to a final 50 ml volume with bi-distilled water. Sodium measurements were done by flame atomic absorption spectroscopy (air/acetylene) using a Unicam spectrophotometer model 969. The analysis methodology was validated using certified reference material (BIMEP-432), supplied by the Wageningen Evaluating Programs for Analytical Laboratories (WEPAL). The reagents used were of high purity (Suprapur, Merck, Darmstadt, Germany) and the standard solutions for the various metals were prepared from concentrated solutions (Fisher Scientific International Company).

2.13. Statistical analysis

All data was subjected to different types of statistical analyses by using the software R and Rcmdr package (http://knuth.uca.es/R/doku.php?id=instalacion_de_r_y_rcmdr:r-uca). They included t-student (endocytosis rate, plant biomass and ROS quantification), one way ANOVA (signal fluorescence of sodium green quantification and sodium contents in roots and shoots). Statistical differences are referred to as significant when $P \leq 0.05$.

3. Results

3.1. Identification and isolation of GDP dissociation inhibitor gene SchRabGDI1 from Solanum chilense

Subtractive cDNA hybridization of stressed (salt-treated) and unstressed plants (control treatment) of *S. chilense* was carried out to isolate differentially up-regulated genes in response to salt stress. This strategy identified several genes and their sequences were compared with the NCBI database since no annotation is available for the *S. chilense* genome. One of these genes, named *SchRabGDI1* (Accesion number AY787206), showed high similarity to a GDP dissociation inhibitor (GDI) gene from *Solanum lycopersicum*. The full-length clone of *SchRabGDI1* (1335 nucleotides) encodes a protein of 444 amino acid residues. A search conducted in the Solgenomic database (https://solgenomics.net/) predicted three putative RabGDI genes in the genome of the cultivated tomato (*S. lycopersicum*), which were named SlGDI1, SlGDI8 and SlGDI12 according to their chromosome location.

The deduced protein sequence of *SchRabGDI1* was 99% identical to SlGDI12 (Solyc12g017570.1) from *S. lycopersicum* and StGDI (NP_001274860.1) from *S. tuberosum*. The amino acid sequence similarity to other GDIs were: 93.5% with SlGDI8 (Solyc08g015860.2), 84.41% with AtGDI1, 84.23% with AtGDI2 and 82.21% with SlGDI1 (Solyc01g105810.2). At the structural level, *SchRabGDI1* presented five classical domains of the GDIs called SCR (Sequence Conserved Regions), composed of invariant sequences of tri or tetra peptides (Fig. S1A). The phylogenetic analysis revealed that *SchRabGDI1* is closely associated with GDI proteins from the Solanacea family, such as those of *S. tuberosum* RabGDI, *S. lycopersicum* RabGDI12 and RabGDI8 and *Nicotiana tabacum* RabGDI1 (AAB80717; [50]), whereas RabGDI1 from *S. lycopersicum* grouped separately from the rest of the plant RabGDI proteins (Fig. S1B). These results strongly suggested that *SchRabGDI1* encodes a RabGDI in wild tomato *S. chilense*.

3.2. SchRabGDI1 is induced under salt stress in S. chilense

Due to the genetic redundancy of *RABGDIs* in plants, we studied the organ-specific transcriptional profile of *SchRabGDI1*. When *S. chilense* plants were grown under control conditons, *SchRabGDI1* expression was detected in all the analyzed tissues (Fig. 1), being its transcript levels slightly higher in roots than in flowers and other vegetative tissues (Fig. 1). To assess the inducibility of *SchRabGDI1* by salt, *S. chilense* plants were exposed to a severe salt stress treatment (400 mM NaCl) and the expression patterns of *SchRabGDI1* and two stress-responsive genes *TSW12* [32,51] and *AREB1* [32,52] were analyzed. An increase in the transcript levels of *SchRabGDI1* were observed in roots 3 h after treatment (Fig. 2**A**), reaching a maximum level (4-fold) at 6 h and then decreased gradually to control levels after 72 h. In leaves, up-regulation of *SchRabGDI1* was detected 3 h after treatment, with the highest expression levels (4-fold) attained 12 h after treatment, declining to basal levels after 24 h and remained constant thereafter (Fig. 2**B**). *SchRabGDI1* expression pattern under salt stress was similar to the profile displayed by the stress-induced genes *TSW12* and *AREB1* (Fig. 2**C** and **D**), suggesting that they may respond to a similar signaling pathway and a possible participation of this RabGDI protein in mechanisms associated with stress response.

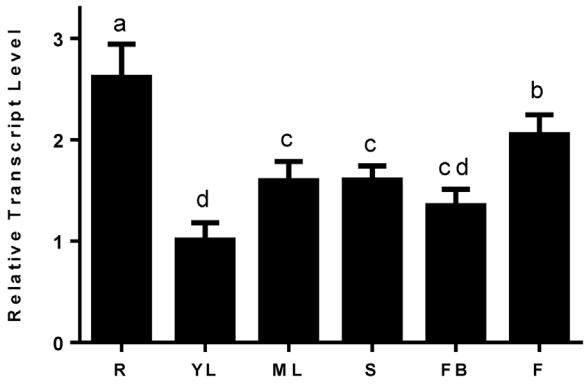

Fig. 1. Gene expression profile of *SchRabGDI1* in vegetative and reproductive tissues of *S. chilense*. The relative abundance of the transcripts was determined by qPCR from total RNA of the indicated organs: **R** root, **T** stem, **YL** Young leaf, **ML** mature leaf, **FB** floral buttons and **F** flowers. Values represent mean ± SE (n = 3). The constitutive expression of the gene *SchUBI3* and the 2-ΔΔCt method described by [31] were used for normalization. The transcript levels obtained for YL were taken to assign the value one.

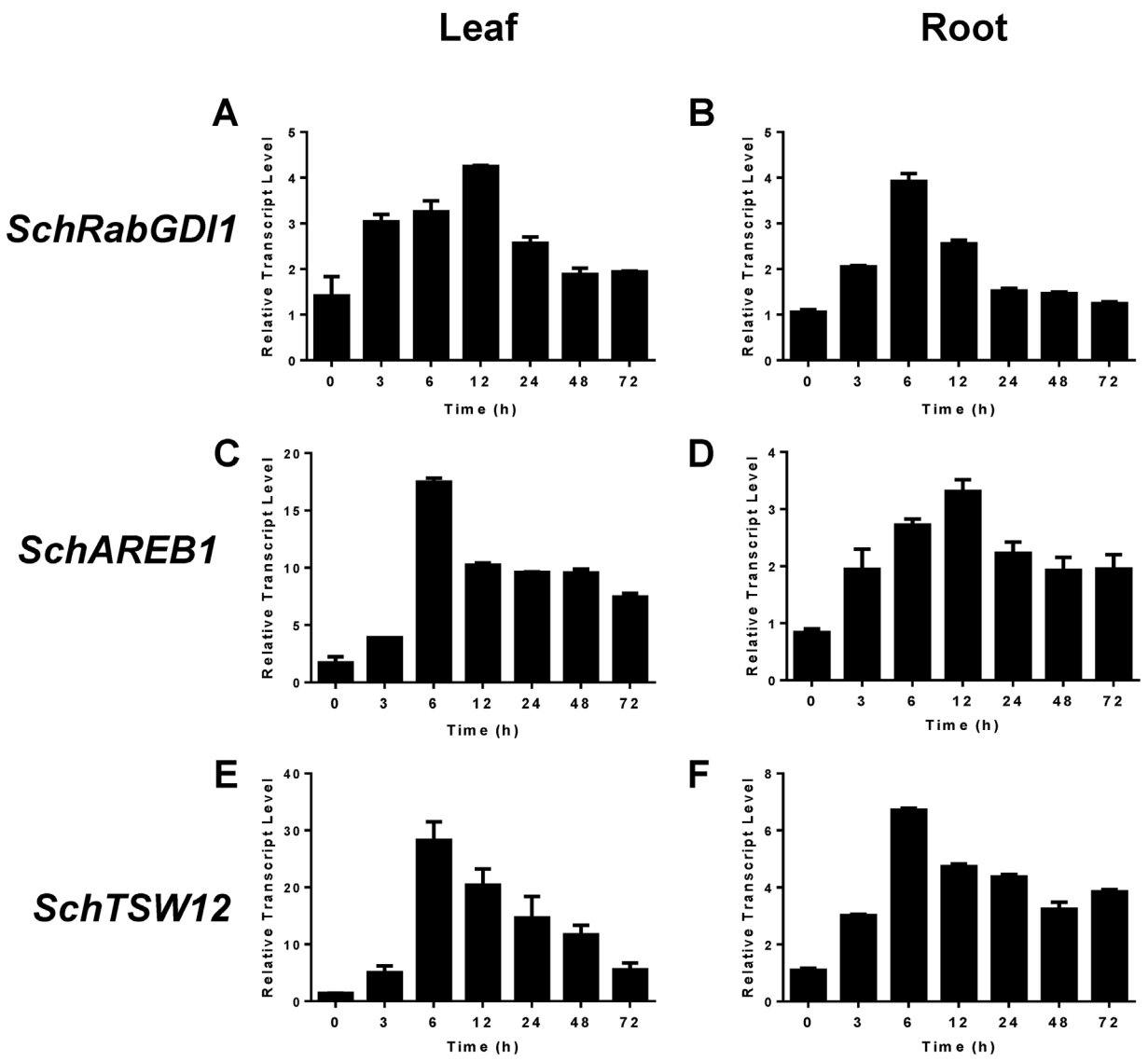

Fig. 2. Expression analysis of *SchRabGDI1* in *S. chilense* exposed to salt stress. *SchRabGDI1* (**A, B**), *SchAREB1* (**C, D**) and *SchTSW12* (**E, F**), were evaluated by qRT-PCR using total RNA extracted from leaves and roots of 12 weeks old plants after salt stress treatment (300 mM NaCl) for a period of 0, 3, 6, 12, 24, 48 and 72 h. Values are the mean ± SE (n = 3). Expression of the constitutive gene *SchUBI3* and the 2-ΔΔCt method described by [31] were used for normalization. The transcript levels obtained in roots at time 0 were assign the value of one for each gene analyzed.

3.3. SchRabGDI1 encodes a RabGDI protein

Functional characterization of *SchRabGDI1* was carried out by functional complementation of a yeast mutant with a defect in membrane trafficking. *S. cerevisiae* contains a single copy gene encoding a Rab-GDP dissociation inhibitor (*GDI1*) which is allelic to the *SEC19* gene [53,54]. Mutations in *SEC19* (*i.e.* the *sec19-1* mutation) cause a thermosensitive growth defect, thus allowing the *sec19* mutant strain to grow at a permissive temperature (25 °C) but not at the restrictive temperature of 37 °C. The *sec19-1* mutant was transformed with the construct *GAL1:SchRabGDI1*, which allows to switch on and off the expression of the *SchRabGDI1* by adding galactose or glucose in the media, respectively. *SchRabGDI1* expression rescued the defective mutant phenotype at 37 °C in a medium containing galactose (Fig. 3). However the mutant transformed with *GAL1:SchRabGDI1* still displayed a growth defect at 37 °C in glucose-containing media which repressed the GAL1 promoter. Therefore these results demonstrated that *SchRabGDI1* encoded a functional RabGDI protein able to restore the function of a defective *SEC19* gene in *S. cerevisae.*

3.4. SchRabGDI1 interacts with SchRabG3e in vivo

RabGDIs are regulatory proteins that interact with RabGTPases and mediate their recycling [4]. In addition to *SchRabGDI1*, we identified and isolated a *SchRabG3e* which is identical to *AtRabG3e* from *Arabidopsis thaliana*. *In silico* analysis predicted the interaction between *SchRabGDI1* and SchRabG3e (Fig. 4**A**). Protein-protein docking between the tri-dimensional structures of *SchRabGDI1* and SchRabG3e and the structural alignment with the RabGTPase-RabGDI crystalized structure PDB code 1UKV, showed the binding platform between both proteins (Figs. S1A and S2). Indeed, the molecular dynamics analysis revealed the essential residues that participate in the interaction interface (Figs. S1A and S2). To confirm that these two proteins can interact *in vivo,* we followed a bimolecular fluorescence complementation (BiFC) assay which is based on the restoration of fluorescence after two fluorescent protein halves are brought together due to the protein-protein interaction of two proteins of interest fused to the fluorescent halves [55]. To develop the assay, we first evaluated (*in silico)* the effect that fusion proteins could have on RabGTPase-RabGDI binding. Visual evaluation of the structures formed by the half of the fluorescent

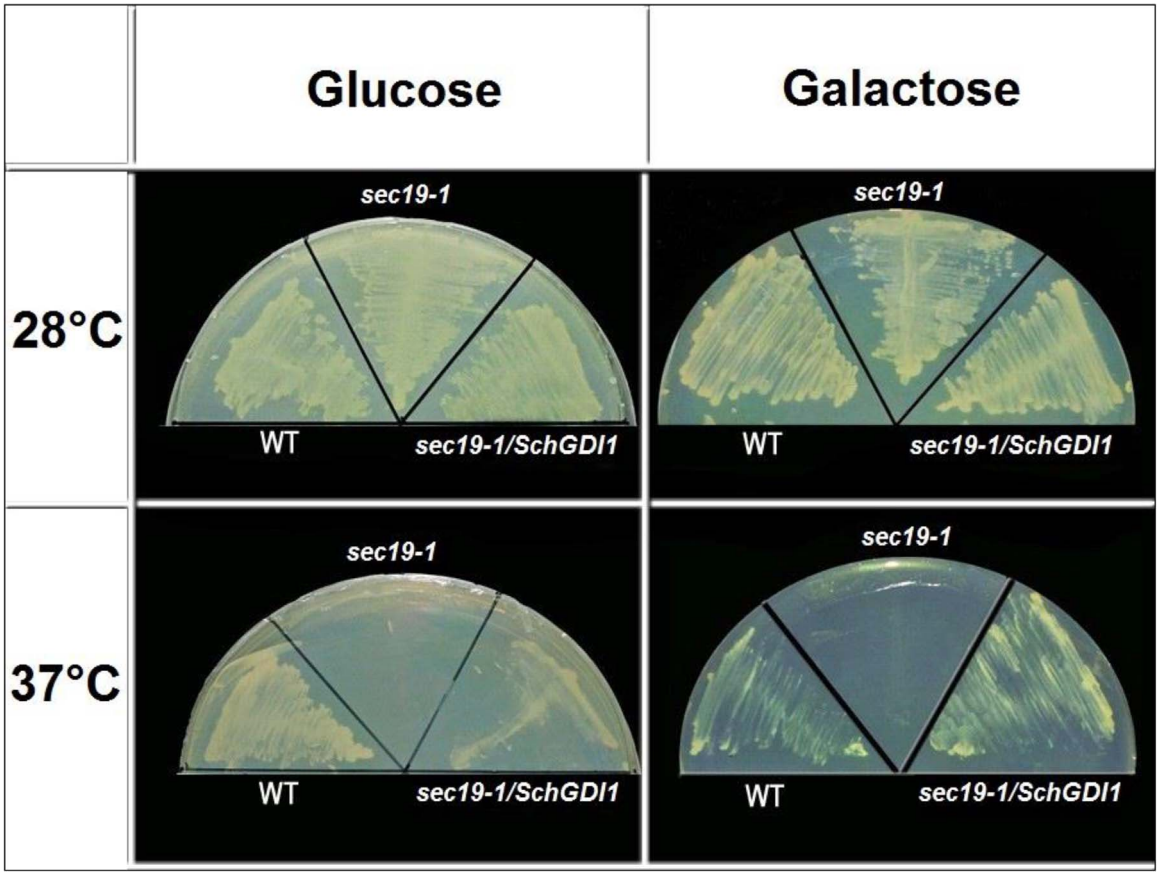

Fig. 3. Complementation assay of the *sec19* yeast strain with *SchRabGDI1*. RSY249 (WT) and RSY274 (*sec19-1*) yeast cells were transformed with pYES-DEST52 and *sec19-1* (*gdi1*) cells transformed with *GAL1:SchRabGDI1* were streaked on glucose (Gluc; SC-URA) and galactose (Gal; SC-URA) plates and incubated at 37 °C (restrictive) and 28 °C (permissive) for 3 days.

protein Venus fused to the C-terminal end of *SchRabGDI1* and half of the super cyan fluorescent protein (SCFP) bound to the free N-terminal end of SchRabG3e, together with a molecular dynamics analysis of each system, indicated that there was no obstruction of the RabGTPase-RabGDI binding platform (Fig. 4**B**). Subsequently, the constructs GDI-VYNE (*SchRabGDI1* fused to the N-terminal half of Venus) and SCYCE-RabG3e (C-terminal half of SCFP fused to N-terminal of SchRabG3e) were transiently expressed in epidermal cells of tobacco (*Nicotiana benthamiana*) leaves. As a positive control of the transformation, a construct that allows the accumulation of the plasma membrane intrinsic protein PIP1;4 fused to red fluorescent protein (PIP1:4-RFP) was also used. The green fluorescence signal showed the interaction

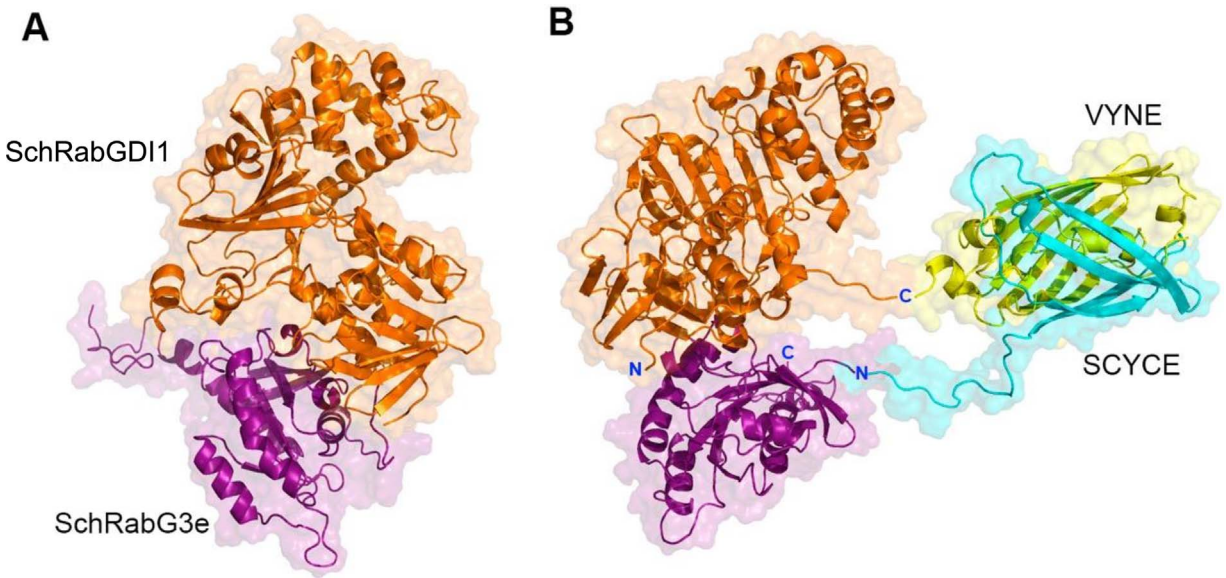

Fig. 4. Structural docking between *SchRabGDI1*, SchRabG3e and fusion proteins. **(A)**The energy of protein-protein docking *SchRabGDI1*-SchRabG3e calculated by the CLUSPRO software was −693 Kcal/mol. **(B)** Complex of Rab-GDI-YC155-YN155 proteins. It is presented to VYNE (yellow) fused to the C-terminus end of *SchRabGDI1* (orange) and SCYCE (cyan) fused to the N-terminus of SchRabG3e (purple). (For interpretation of the references to colour in this figure legend, the reader is referred to the web version of this article.)

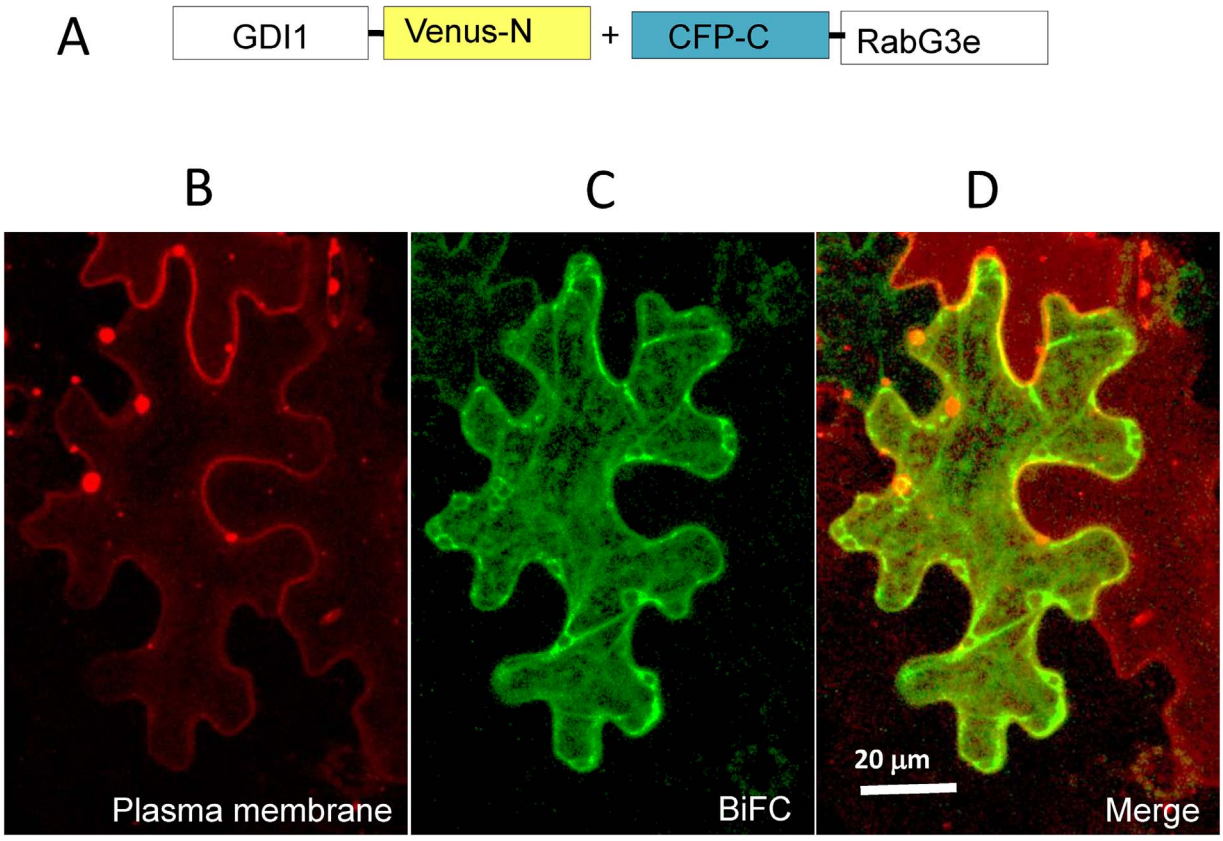

Fig. 5. BiFC interaction of *SchRabGDI1* and SchRabG3e in tobacco leaf epidermal cells. Scheme of the fusion constructs used in BiFC (A). Representative fluorescent images showing RFP signal of the plasma membrane intrinsic protein 1–4 (PIP1;4) (B), BiFC-signal of *SchRabGDI1* and SchRabG3e (C) and merged pictures (D) Protein-protein interaction shown in C, was performed using the genetic constructions pDEST-GDI1:VYNE and pDEST-SCYCE:RabG3e. Figure represents the maximum projection of Z-stacks of 14 slices.

between GDI-VYNE and SCYCE-RabG3e fusion proteins confirming the *in vivo* interaction of *SchRabGDI1* and SchRabG3e (Fig. 5). In both constructs, the *SchRabGDI1* and SchRabG3e maintained their own targeting sequences for their localization. The endosome-like and membrane-like pattern of green fluorescent *SchRabGDI1*-SchRabG3e complex was consistent with the molecular function of the complex in membrane recruiting, supporting the role of *SchRabGDI1* in endomembrane trafficking (Fig. 5). To verify that the interaction of *SchRabGDI1* and SchRabG3e was specific, AtNHX5 which is known to localize in endosomal compartments [46] was used as negative control for the interaction with SchRabG3e. As shown in Fig. S3B, BiFC signal of AtNHX5 and SchRabG3e was not observed, while the plasma membrane expression control showed fluorescence signal of RFP. Similarly, Fig. S3C showed no BiFC signal of *SchRabGDI1* and AtRem1.2 (encoding Remorin, a membrane raft-bound protein) interaction. BiFC signal of AtNHX5 and AtRem1.2 in Fig. S3D showed that the NHX5-VYNE and SCYCE-Rem1.2 genes were properly expressed and interacted. These results indicated that the BiFC interaction between *SchRabGDI1* and SchRabG3e was specific.

3.5. Expression of SchRabGDI1 in Arabidopsis enhances tolerance to salt stress

Given the salt-induced *SchRabGDI1* expression in *S. chilense* (Fig. 2), we assessed whether the heterologous expression of *SchRabGDI1* could contribute to enhance salt tolerance in *Arabidopsis thaliana*. Homozygous T3 transgenic Col-0 Arabidopsis overexpressing *SchRabGDI1* were generated (Fig. S4) and their growth performance under 75 mM NaCl was tested (Fig. 6). No phenotypical differences were observed when the plants were grown under control conditions and their biomass was not affected (Fig. 6**A**). On the other hand, when plants were subjected to 75 mM NaCl, growth of transgenic plants expressing higher levels of *SchRabGDI1* (L15 and L32) (Fig. S5) was less affected (Fig. 6**B**). Salt stress induces the accumulation of toxic reactive oxygen species (ROS) (Miller et al., 2010). Histochemical staining with nitroblue tetrazolium (NBT) showed that transgenic lines L15 and L32 accumulated less superoxide radical (O_2^-) than wild type plants after salt treatment (Fig. 7). The results showed that the salt tolerance displayed by the transgenic plants correlated with *SchRabGDI1* expression levels (Figs. 7**B** and S4), strongly suggesting an active role of *SchRabGDI1* in stress tolerance. Besides, the total Na^+ content was determined before and after salt treatment. The content of Na^+ in shoot and roots from transgenic and WT plants was similar before the salt treatment however after the treatment, the shoot Na^+ content in the transgenics was lower than in WT, while the root Na^+ content was higher than in WT (Fig. 8**A** and **B**).

3.6. Endocytosis is induced by expressing SchRabGDI1 in Arabidopsis

To analyze the involvement of *SchRabGDI1* in the endocytic pathway, Arabidopsis transgenic plants overexpressing *SchRabGDI1* were used to monitor endocytosis by using the endocytic tracer dye FM4-64 [56] which initially binds the plasma membrane and then is internalized to endosomes. Fig. 9 shows FM4-64 internalization at 5 and 30 min in root cells of wild-type (control) and *SchRabGDI1* transgenic lines. An enhanced internalization of FM4-64 was already observed at 5 min after the endocytosis time course in *SchRabGDI1* transgenic lines compared to the wild-type (Fig. 9**A**). The increased internalization of the tracer dye was evidenced by the higher abundance of small punctate FM4-64-endosomes at both 5 and 30 min of endocytosis dynamics. Quantification of the FM4-64 fluorescence signal showed significant differences in the endocytic rates between wild-type and overexpressing *SchRabGDI1* lines (~15%) (Fig. 9**B**), suggesting that an increment in the cellular RabGTPases pool brought about by

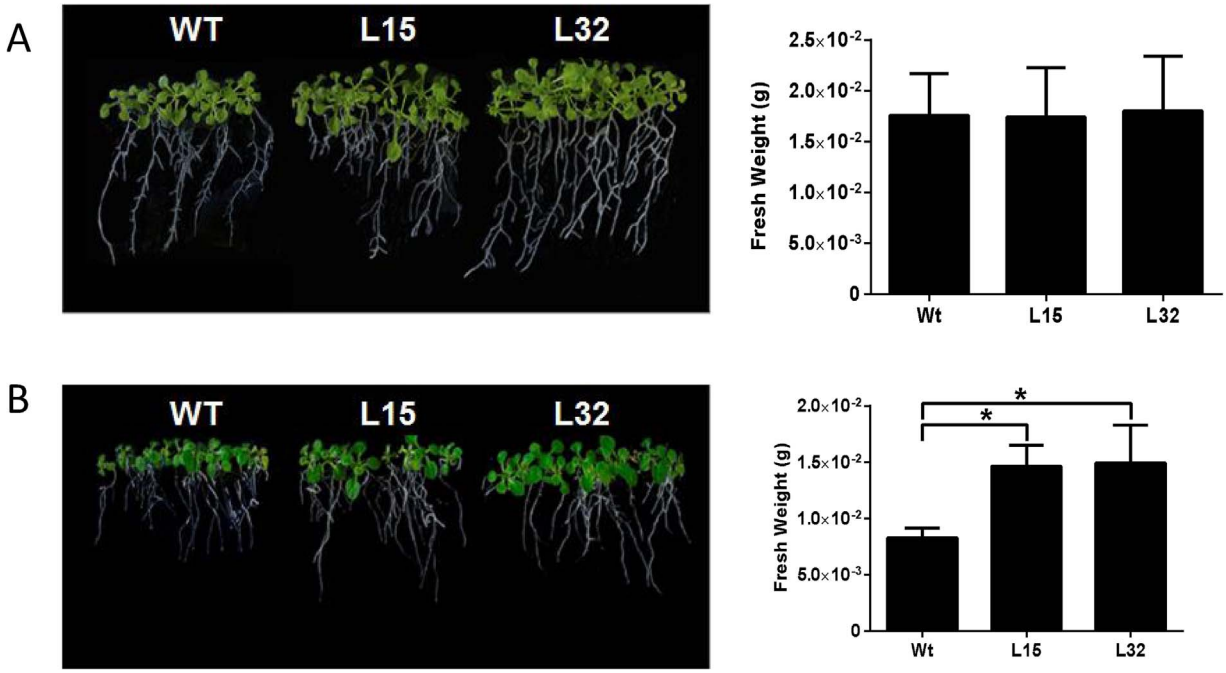

Fig. 6. Analysis of Arabidopsis plants expressing *SchRabGDI1* subjected to salt stress. Phenotypes and fresh weight of transgenic lines expressing *SchRabGDI1* under normal growth condition (MS) (**A**) and 75 mM NaCl (**B**). Three independent experiments with five plants of each genotype were used in the analysis. Data are the mean +/− S.D. (n = 3). Asterisks represent significant difference from the wild type ($P < 0.05$).

SchRabGDI1 increased the rate of endocytic trafficking,evidencing the cellular functionality of *SchRabGDI1*.

In addition, the intracellular Na^+ distribution in root cells of wild type and *SchRabGDI1* transgenic lines subjected to 100 mM NaCl was monitored using the fluorescent Na^+ indicator Sodium Green and the endocytic tracer FM4-64. Fig. S5 shows root cells from the transition zone in which Na^+ ions are deteced in the lumen of the main vacuole and smaller vesicular structures (Fig. S5A). Quantification of the fluorescence intensity of Sodium Green revealed a higher accumulation of Na^+ in the transgenic lines compared to wild type (Fig. S5B). These results indicate that the increase in salt tolerance conferred by over-expression of *SchRabGDI1* may be consequence of an intensification of endocytosis and sodium accumulation in root cells.

4. Discussion

The physiological response of plants to salt stress is a complex process that requires the coordinated function of many genes. Although members of the *Rab* family genes has been associated to endosomal trafficking [57], little is known about the participation of those associated with the control of the molecular switch of RabGTPases in the response to saline stress. In this work, we report that *SchRabGDI1*, one of the genes involved in the control of cycling between active and inactive state of Rab proteins, plays a role in the tolerance of plants to salt stress.

4.1. SchRabGDI1 encodes a functional GDP dissociation inhibitor and is induced by salt stress

SchRabGDI1 was identified among salt stress-induced transcripts of *Solanum chilense* roots. *SchRabGDI1* expression was induced early by salinity in both leaves and roots as two stress-responsive genes *TSW12* [32,51] and *AREB1* [32,52] (Fig. 2). *SchRabGDI1*expression patterns was similar to that of *AtRabGDI1*(AT2G44100) in Arabidopsis (http://bar.utoronto.ca/efp/cgi-bin/efpWeb.cgi), but differed to the expression of *RabGDI* from *Mangifera indica L*, which is down-regulated in leaves

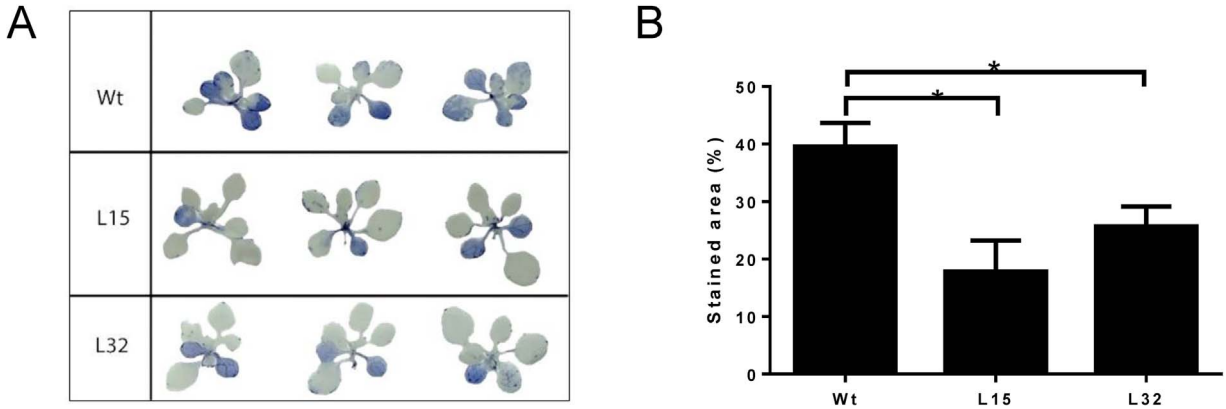

Fig. 7. ROS accumulation in wild-type and Arabidopsis plants expressing *SchRabGDI1* under salt stress. (**A**) ROS accumulation was evaluated on seedlings of wild-type and three transgenic lines (4 weeks-old) exposed under normal (MS) or saline media (MS + 100 mM NaCl) during 15 days. Fifteen seedlings were used for each line, and three representative pictures of each line are shown. (**B**) Quantification was performed using the software image J. from fifteen plants per line. Values are mean +/− S.E. (n = 15). Asterisks represent significant difference from the wild type ($P < 0.05$).

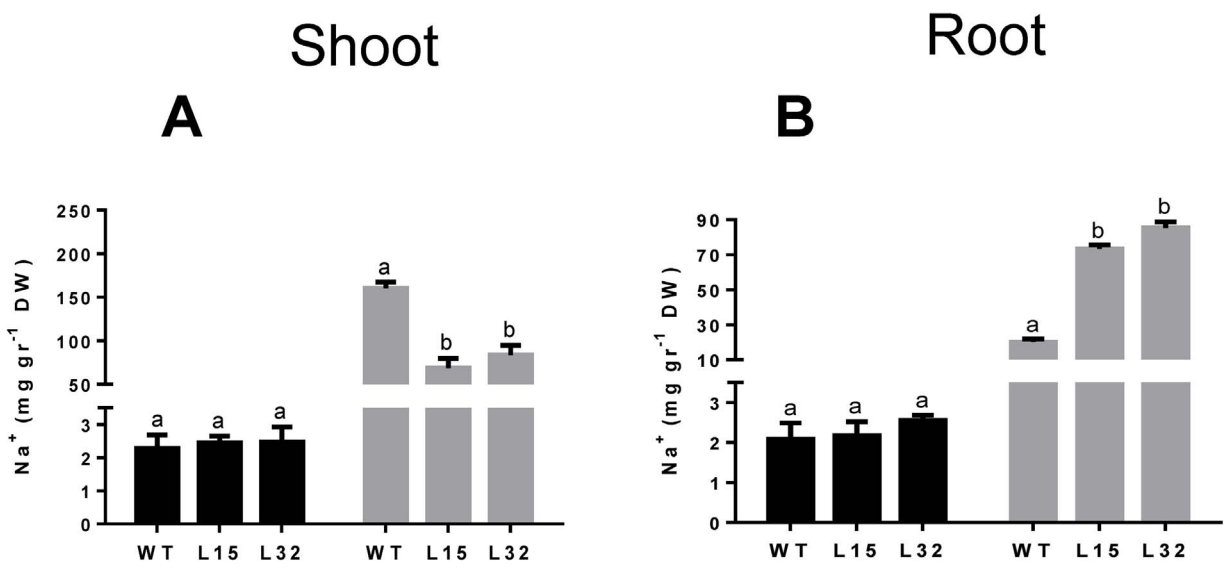

Fig. 8. Total Na^+ content in shoots and roots of Arabidopsis. Fifteen-day-old seedlings of wild-type (Col-0) and transgenic lines (*SchRabGDI1*) were subjected to control conditions and salt stress with 75 mM NaCl. Total sodium content from shoots and roots are showed in **A** and **B**, respectively. Solid and grey bars represent Na^+ content before and after the treatment, respectively. Values are mean +/− S.E. (n = 15). The bars with different letters are significantly different from each other ($P < 0.05$).

under similar salt stress conditions [58]. However, the timing of the induction of *SchRabGDI1* in response to such stimulus coincides with that described for genes that belong to the RabGTPase family such as *McRab5-b* from *Mesembryanthemum crystallinum* [56], *AtRabG3e* (AT1G49300.1) and *AtRabA1*(At1g06400) from *Arabidopsis thaliana* [22,24], (http://bar.utoronto.ca/efp/cgi-bin/efpWeb.cgi) and *SchRabG3e* from *S. chilense* (data not shown). These results would suggest that *SchRabGDI1* expression is required during the vesicular trafficking events occuring during salt stress.

The analysis of the deduced amino acid sequence showed that

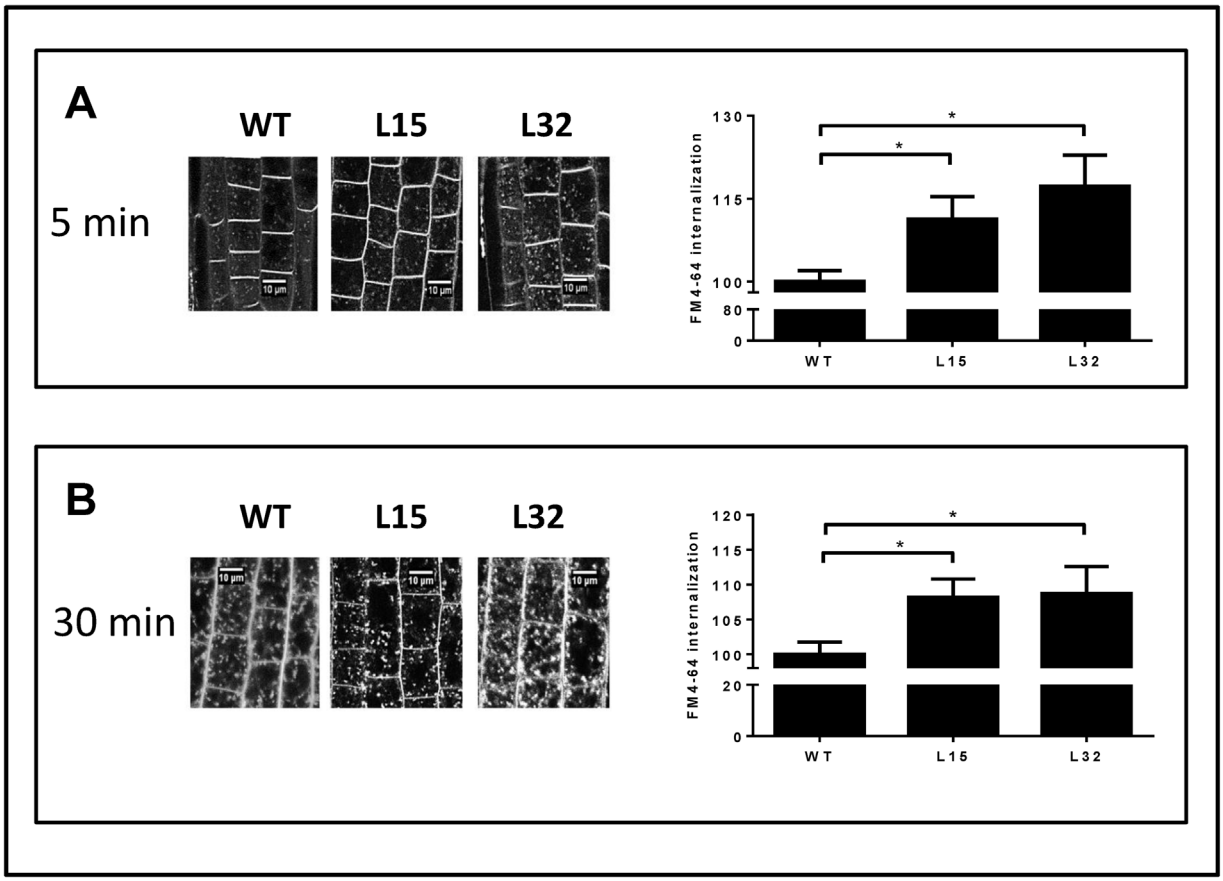

Fig. 9. Endocytosis in wild-type and transgenic cell roots expressing *SchRabGDI1*. Membrane internalization was visualized using the tracer FM4-64 in root cells of 7day-old seedlings and the confocal images were captured at 5 min (A) and 30 min (B) after staining. Scale bar = 10 µm. The fluorescence quantification was performed using the FIJI-Image J software Schindelin et al. [48]. The rate of FM4-64 internalization was calculated by the ratio between the mean of the intracellular fluorescence and the mean of the whole cell fluorescence (including the plasma membrane) from 20 to 50 cells. Three biological and three technical replicates were performed.

SchRabGDI1 possesses high sequence similarity with other RabGDI from plants and its evolutionary proximity to RabGDIs of *S. tuberosus*, *S. lycopersicum* and *Nicotiana tabacum* (Fig. S1B). *SchRabGDI1* contains the five domains that structurally and functionally define sequence conserved residues (SCRs) which are characteristic of all RabGDIs (Fig. S1A). Functionally, *SchRabGDI1* was able to complement the yeast secretory mutant *sec19* RSY273, restoring the lethal temperature-sensitive phenotype [53].

Protein-protein interaction between Rab and GDI proteins is critical for maintaining an efficient vesicular trafficking, since GDI retrieves the GDP-bound form of Rab from the membrane to form a heterodimeric complex that is used as a cytosolic pool for the reuse of inactive Rab during a series of vesicle budding and fusion [4,59]. We used bioinformatics tools to determine the essential residues for the interaction of *SchRabGDI1* and SchRabG3e, which revealed a high interaction affinity with very low ΔG (Figs. 4 **A** and S2). The results obtained using bimolecular fluorescence complementation (BiFC) assays ratified the *in silico* predictions given that the *in vivo* interaction between *SchRabGDI1* and SchRabG3e was observed when both genes were transiently co-expressed in epidermal cells of tobacco leaves (Fig. 5). This demonstrated that *SchRabGDI1* was able to form a heterodimer with SchRabG3e, suggesting its functional participation in the cycle of RabGTPases and their likely involvement in intracellular vesicular trafficking.

4.2. SchRabGDI1 confers tolerance to saline stress in Arabidopsis

In recent years, evidences indicate that intracellular vesicular traffic plays an important role in the adaptation of plants to salt stress [21,60]. Ectopic expression and silencing have been used to show that members of *Rab GTPases* and *SNARES* (soluble N-ethylmaleimide sensitive factor attachment protein receptor) families, two major regulators of vesicular trafficking, participates in the tolerance of plants to salt stress [22,24,61–64]. Under standard growth conditions wild and transgenic plants do not exhibit a differential phenotype (Fig. 6A), probably because the protein encoded by the transgene requires the expression of the other genes that constitute the molecular switch of RabGTPases, which are not expressed under this conditions.To demonstrate its involvement in the response to salt stress, we analyzed the effect of ectopic expression of *SchRabGDI1* in Arabidopsis plants. Transgenic plants showed increased tolerance to salt (75 mM NaCl), displaying higher fresh weight and reduced accumulation of reactive oxygen species compared to wild type plants (Figs. 6 and 7). The improved salinity tolerance of Arabidopsis plants harboring *SchRabGDI1* is comparable to results described in Arabidopsis, tobacco and rice overexpressing *Rab7* (*RabG3e*) when exposed to salt stress [22,23,65]. In addition to accumulate Na^+ into their vacuoles and to extrude Na^+ to the apoplast, plants also restrict the movement of Na^+ ion from the roots to the shoots [19]. The enhanced salt tolerance displayed by the transgenic plants overexpressing *SchRabGDI1* correlated with the increased Na^+ accumulation in the root vacuoles and the differential Na^+ content between roots and shoots.

4.3. SchRabGDI1 regulates endocytic pathway and Na^+ intracellular distribution

Leshem et al. [66] reported that salt stress induced bulk-flow endocytosis in Arabidopsis roots. The increased endocytosis induced by salt stress has been confirmed subsequently in other studies [60,67,68]. The bulk endocytosis induced by salt has been shown to promote a rapid increase in vacuolar volume and accumulation of sodium in the vacuole of roots cells [20]. In this work, the overexpression of *SchRabGDI1* in Arabidopsis roots led to an increase in endocytosis as determined by the tracer dye FM 4–64 (Fig. 8). Moreover, when exposed to 100 mM NaCl, the transgenic plants showed higher accumulation of sodium in their root vacuoles (as measured by the fluorescence of the dye sodium-green) (Fig. S4). These results suggest the participation of *SchRabGDI1* in the regulation of endocytosis and postulates a possible contribution of salt-induced endocytosis to sodium accumulation in the vacuole, in addition to the action of vacuolar Na^+/H^+ antiporters [19,69]. In conclusion, our findings suggest that salt tolerant species such as *S. chilense* use bulk endocytosis as one of the early mechanisms to avoid the saline stress, for which they require the concerted expression of regulatory genes of the vesicular trafficking of the endocytic pathway.

Funding source

This work was supported by Fondo Nacional de Desarrollo Científico y Tecnológico (FONDECYT, grant number 1140636). A.SM. was supported by fellowships from Comisión Nacional de Investigación Científica y Tecnológica (CONICYT-Chile); F.S. and J.M-E. were supported by Universidad de Talca fellowships. H.T. was supported by the Will W. Lester Endowment of the University of California.

Acknowledgement

We thank Dr. José Casaretto (Department of Molecular and Cellular Biology, University of Guelph) for critical reading of the manuscript.

Appendix A. Supplementary data

Supplementary data associated with this article can be found, in the online version, at http://dx.doi.org/10.1016/j.plantsci.2017.06.007.

References

[1] P. Chavrier, B. Goud, The role of ARF and Rab GTPases in membrane transport, Curr. Opin. Cell Biol. 11 (1999) 466–475.
[2] J.B. Pereira-Leal, M.C. Seabra, The mammalian Rab family of small GTPases: definition of family and subfamily sequence motifs suggests a mechanism for functional specificity in the Ras superfamily, J. Mol. Biol. 301 (2000) 1077–1087.
[3] S. Wu, K. Zeng, A. Wilson, W.E. Balch, Structural insights into the function of the Rab GDI superfamily, Trends Biochem. Sci. 21 (1996) 472–476.
[4] S.R. Pfeffer, A.B. Dirac-Svejstrup, T. Soldati, Rab GDP dissociation inhibitor: putting rab GTPases in the right place, J. Biol. Chem. 270 (1995) 17057–17059.
[5] V. Vernoud, A.C. Horton, Z. Yang, E. Nielsen, Analysis of the small GTPase gene superfamily of arabidopsis, Plant Physiol. 131 (2003) 1191–1208.
[6] A.V. Andreeva, M.A. Kutuzov, D.E. Evans, C.R. Hawes, Rab-GDP dissociation inhibitor isoforms in Arabidopsis thaliana, J. Exp. Bot. 48 (1997) 2109–2110.
[7] T. Ueda, N. Matsuda, T. Anai, H. Tsukaya, H. Uchimiya, A. Nakano, An Arabidopsis gene isolated by a novel method for detecting genetic interaction in yeast encodes the GDP dissociation inhibitor of Ara4 GTPase, Plant Cell 8 (1996) 2079–2091.
[8] T. Ueda, T. Yoshizumi, T. Anai, M. Matsui, H. Uchimiya, a Nakano AtGDI2, a novel Arabidopsis gene encoding a Rab GDP dissociation inhibitor, Gene 206 (1998) 137–143.
[9] W. Yeon, C.Y. Kim, N.E. Cheong, Y.O. Choi, K.O. Lee, S. Lee, J.B. Park, A. Nakano, J.D. Bahk, M.J. Cho, Characterization of two fungal-elicitor-induced rice cDNAs encoding functional homologues of the rab-specific, Planta 210 (1999) 143–149.
[10] B. Ezaki, M. Koyanagi, R.C. Gardner, H. Matsumoto, Nucleotide sequence of a cDNA for GDP dissociation inhibitor (GDI) which 1 s induced by aluminum (Al) ion stress in tobacco cell culture, Plant Physiol. 115 (1997) 313–315.
[11] F.J. Muñoz, R. Esteban, E. Labrador, B. Dopico, Expression of a novel chickpea Rab-GDI cDNA mainly in seedlings, Plant Physiol. Biochem. 39 (2001) 363–366.
[12] P. Abbal, C. Tesniere, Putative Vitis vinifera Rop- and Rab-GAP- GEF-, and GDI-interacting proteins uncovered with novel methods for public genomic and EST database analysis, J. Exp. Bot. 61 (2010) 65–74.
[13] J.B. Heo, Y.B. Yi, J.D. Bahk, Rice GDP dissociation inhibitor 3 inhibits OsMAPK2 activity through physical interaction, Biochem. Biophys. Res. Commun. 414 (2011) 814–819.
[14] P. D'Adamo, a Menegon, C. Lo Nigro, M. Grasso, M. Gulisano, F. Tamanini, T. Bienvenu, a K. Gedeon, B. Oostra, S.K. Wu, a Tandon, F. Valtorta, W.E. Balch, J. Chelly, D. Toniolo, Mutations in GDI1 are responsible for X-linked non-specific mental retardation, Nat. Genet. 19 (1998) 134–139.
[15] I.A. Yaneva, K. Niehaus, Molecular cloning and characterisation of a Rab-binding GDP-dissociation inhibitor from Medicago truncatula, Plant Physiol. Biochem. 43 (2005) 203–212.
[16] R. Munns, M. Tester, Mechanisms of salinity tolerance, Ann Rev. Plant Bio. 59 (2008) 651–681.
[17] F.J.M. Maathuis, Sodium in plants: perception, signalling, and regulation of sodium fluxes, J. Exp. Bot. 65 (2014) 849–858.
[18] E. Blumwald, R.J. Poole, Salt tolerance in suspension cultures of sugar beet:

induction of na/h antiport activity at the tonoplast by growth in salt, Plant Physiol. 83 (1987) 884–887.
[19] E. Blumwald, Sodium transport and salt tolerance in plants, Curr. Opin. Cell Biol. 12 (2000) 431–434.
[20] T. Mimura, M. Kura-Hotta, T. Tsujimura, M. Ohnishi, M. Miura, Y. Okazaki, M. Mimura, M. Maeshima, S. Washitani-Nemoto, Rapid increase of vacuolar volume in response to salt stress, Planta 216 (2003) 397–402.
[21] K. Hamaji, M. Nagira, K. Yoshida, M. Ohnishi, Y. Oda, T. Uemura, T. Goh, M.H. Sato, M.T. Morita, M. Tasaka, S.-i. Hasezawa, A. Nakano, I. Hara-Nishimura, M. Maeshima, H. Fukaki, T. Mimura, Dynamic aspects of ion accumulation by vesicle traffic under salt stress in arabidopsis, Plant Cell Physiol. 50 (2009) 2023–2033.
[22] A. Mazel, Y. Leshem, B.S. Tiwari, A. Levine, Induction of salt and osmotic stress tolerance by overexpression of an intracellular vesicle trafficking protein AtRab7 (AtRabG3e), Plant Physiol. 134 (2004) 118–128.
[23] P.K. Agarwal, P. Agarwal, P. Jain, B. Jha, M.K. Reddy, S.K. Sopory, Constitutive overexpression of a stress-inducible small GTP-binding protein PgRab7 from Pennisetum glaucum enhances abiotic stress tolerance in transgenic tobacco, Plant Cell Rep. 27 (2008) 105–115.
[24] R. Asaoka, T. Uemura, J. Ito, M. Fujimoto, E. Ito, T. Ueda, A. Nakano, Arabidopsis RABA1 GTPases are involved in transport between the trans-Golgi network and the plasma membrane, and are required for salinity stress tolerance, Plant J. 73 (2012) 240–249.
[25] A. Baral, N.G. Irani, M. Fujimoto, A. Nakano, S. Mayor, M.K. Mathew, Salt-induced remodeling of spatially restricted clathrin-independent endocytic pathways in Arabidopsis root, Plant Cell 27 (2015) 1297–1315.
[26] J. Cuartero, M.C. Bolarín, M.J. Asíns, V. Moreno, Increasing salt tolerance in the tomato, J. Exp. Bot. 57 (2006) 1045–1058.
[27] R.T. Chetelat, R.A. Pertuzé, L. Faúndez, E.B. Graham, C.M. Jones, Distribution, ecology and reproductive biology of wild tomatoes and related nightshades from the Atacama Desert region of northern Chile, Euphytica 167 (2009) 77–93.
[28] G. Tapia, I. Verdugo, M. Yañez, I. Ahumada, C. Theoduloz, C. Cordero, F. Poblete, E. González, S. Ruiz-Lara, Involvement of ethylene in stress-induced expression of the TLC1.1 retrotransposon from Lycopersicon chilense Dun, Plant Physiol. 138 (2005) 2075–2086.
[29] M. Yáñez, S. Cáceres, S. Orellana, A. Bastías, I. Verdugo, S. Ruiz-Lara, J.A. Casaretto, An abiotic stress-responsive bZIP transcription factor from wild and cultivated tomatoes regulates stress-related genes, Plant Cell Rep. 28 (2009) 1497–1507.
[30] J. Loyola, I. Verdugo, E. González, J.A. Casaretto, S. Ruiz-Lara, Plastidic isoprenoid biosynthesis in tomato: physiological and molecular analysis in genotypes resistant and sensitive to drought stress, Plant Biol. 14 (2012) 149–156.
[31] K.J. Livak, T.D. Schmittgen, Analysis of relative gene expression data using real-time quantitative PCR and the 2ˆ-ΔΔCT Method, Methods 25 (2001) 402–408.
[32] S. Orellana, M. Yañez, A. Espinoza, I. Verdugo, E. González, S. Ruiz-Lara, J.a. Casaretto, The transcription factor SlAREB1 confers drought, salt stress tolerance and regulates biotic and abiotic stress-related genes in tomato, Plant Cell Environ. 33 (2010) 2191–2208.
[33] T. Remans, K. Smeets, K. Opdenakker, D. Mathijsen, J. Vangronsveld, A. Cuypers, Normalisation of real-time RT-PCR gene expression measurements in Arabidopsis thaliana exposed to increased metal concentrations, Planta 227 (2008) 1343–1349.
[34] S.J. Clough, A.F. Bent, Floral dip: a simplified method for Agrobacterium-mediated transformation of Arabidopsis thaliana, Plant J. 16 (1998) 735–743.
[35] M. Biasini, S. Bienert, A. Waterhouse, K. Arnold, G. Studer, T. Schmidt, F. Kiefer, T.G. Cassarino, M. Bertoni, L. Bordoli, T. Schwede, SWISS-MODEL, Modelling protein tertiary and quaternary structure using evolutionary information, Nucl. Acids Res. 42 (2014) 252–258.
[36] A. Rak, O. Pylypenko, T. Durek, A. Watzke, S. Kushnir, L. Brunsveld, H. Waldmann, R.S. Goody, K. Alexandrov, Structure of Rab GDP-dissociation inhibitor in complex with prenylated YPT1 GTPase, Science 302 (2003) 646–650.
[37] D. Wiegandt, S. Vieweg, F. Hofmann, D. Koch, F. Li, Y.-W. Wu, A. Itzen, M.P. Müller, R.S. Goody, Locking GTPases covalently in their functional states, Nat. Commun. 6 (2015) 7773.
[38] J.C. Phillips, R. Braun, W. Wang, J. Gumbart, E. Tajkhorshid, E. Villa, C. Chipot, R.D. Skeel, L. Kal, K. Schulten, Scalable molecular dynamics with NAMD, J. Comput. Chem. 26 (2005) 1781–1802.
[39] M. Schlenkrich, J. Brickmann, An empirical potential energy function for phospholipids: criteria for parameter optimization and applications, Bilogical Membranes, Birkhäuser Boston, 1996, pp. 31–81.
[40] W.L. Jorgensen, J. Chandrasekhar, J.D. Madura, R.W. Impey, M.L. Klein, Comparison of simple potential functions for simulating liquid water, J. Chem. Phys. 79 (1983) 926.
[41] R.A. Laskowski, M.W. MacArthur, D.S. Moss, J.M. Thornton, PROCHECK: a program to check the stereochemical quality of protein structures, J. Appl. Crystallogr. 26 (1993) 283–291.
[42] P.G. Comeau, C.N. Filipescu, R. Kabzems, C. DeLong, Corrigendum to: growth of white spruce underplanted beneath spaced and unspaced aspen stands in north-eastern B.C.-10 year results, For. Ecol. Manage. 34 (2004) 2277–2283, http://dx.doi.org/10.1016/j.foreco.2008.11.023.
[43] M.F. Sanner, Python: a programming language for software integration and development, J. Mol. Graph. Model 17 (1999) 57–61.
[44] W. Humphrey, A. Dalke, K. Schulten, VMD. Visual molecular dynamics, J. Mol. Graph. 14 (1996) 33–38, http://dx.doi.org/10.1016/0263-7855(96)00018-5.
[45] C. Gehl, R. Waadt, J. Kudla, R.-R. Mendel, R. Hänsch, New GATEWAY vectors for high throughput analyses of Protein–Protein interactions by bimolecular fluorescence complementation, Mol. Plant 2 (2009) 1051–1058.
[46] E. Bassil, M. Ohto, T. Esumi, H. Tajima, Z. Zhu, O. Cagnac, M. Belmonte, Z. Peleg, T. Yamaguchi, E. Blumwald, The Arabidopsis intracellular Na+/H+ antiporters NHX5 and NHX6 are endosome associated and necessary for plant growth and development, Plant Cell 23 (2011) 224–239.
[47] M. Reguera, E. Bassil, H. Tajima, M. Wimmer, A. Chanoca, M.S. Otegui, N. Paris, E. Blumwald, pH regulation by NHX-type antiporters is required for receptor-mediated protein trafficking to the vacuole in arabidopsis, Plant Cell 27 (2015) 1200–1217.
[48] J. Schindelin, C.T. Rueden, M.C. Hiner, K.W. Eliceiri, The ImageJ ecosystem: an open platform for biomedical image analysis, Mol. Reprod. Dev. 82 (2015) 518–529.
[49] C.F. Grellet Bournonville, J.C. Díaz-Ricci, Quantitative determination of superoxide in plant leaves using a modified NBT staining method, Phytochem. Anal. 22 (2011) 268–271.
[50] B. Ezaki, R.C. Gardner, Y. Ezaki, H. Matsumoto, Expression of aluminum-induced genes in transgenic arabidopsis plants can ameliorate aluminum stress and/or oxidative stress, Plant Physiol. 122 (2000) 657–665.
[51] S. Torres-Schumann, J.A. Godoy, J.A. Pintor-Toro, A probable lipid transfer protein gene is induced by NaCl in stems of tomato plants, Plant Mol. Biol. 18 (1992) 749–757.
[52] T.H. Hsieh, C.W. Li, R.C. Su, C.P. Cheng, Y.C. Sanjaya, Tsai M.T. Chan, A tomato bZIP transcription factor, SlAREB, is involved in water deficit and salt stress response, Planta 231 (2010) 1459–1473.
[53] M.D. Garrett, J.E. Zahner, C.M. Cheney, P.J. Novick, GDI1 encodes a GDP dissociation inhibitor that plays an essential role in the yeast secretory pathway, EMBO J. 13 (1994) 1718–1728.
[54] P. Novick, C. Field, R. Schekman, Identification of 23 complementation groups required for post-translational events in the yeast secretory pathway, Cell 21 (1980) 205–215.
[55] C.D. Hu, Y. Chinenov, T.K. Kerppola, Visualization of interactions among bZIP and Rel family proteins in living cells using bimolecular fluorescence complementation, Mol. Cell. 9 (2002) 789–798.
[56] S. Bolte, K. Schiene, K. Dietz, Characterization of a small GTP-binding protein of the rab 5 family in Mesembryanthemum crystallinum with increased level of expression during early salt stress, Plant Mol. Biol. 42 (2000) 923–936.
[57] H.Y. Yao, H.W. Xue, Signals and mechanisms affecting vesicular trafficking during root growth, Curr. Opin. Plant Biol. 14 (2011) 571–579.
[58] Z. Liu, C. Luo, L. Li, L. Dong, V. Can, P. Wei, X. He, Isolation, characterization and expression analysis of the GDP dissociation inhibitor protein gene MiRab-GDI from Mangifera indica L, Sci. Hortic. (Amsterdam) 185 (2015) 14–21.
[59] C. Saito, T. Ueda, 1st ed., Chapter 4 Functions of RAB and SNARE Proteins in Plant Life Vol. 274 Elsevier Inc., 2009, pp. 183–233.
[60] A. Baral, K.S. Shruthi, M.K. Mathew, Vesicular trafficking and salinity responses in plants, IUBMB Life 67 (2015) 677–686.
[61] Y.S. Son, C.H. Im, D.W. Kim, J.D. Bahk, OsRab11 and OsGAP1 are essential for the vesicle trafficking of the vacuolar H+-ATPase OsVHA-a1 under high salinity conditions, Plant Sci. 198 (2013) 58–71.
[62] J. Zhu, Z. Gong, C. Zhang, C.-P. Song, B. Damsz, G. Inan, H. Koiwa, J.-K. Zhu, P.M. Hasegawa, R. a Bressan, OSM1/SYP61: a syntaxin protein in Arabidopsis controls abscisic acid-mediated and non-abscisic acid-mediated responses to abiotic stress, Plant Cell 14 (2002) 3009–3028.
[63] V.N. Tarte, H.Y. Seok, D.H. Woo, D.H. Le, H.T. Tran, J.W. Baik, I.S. Kang, S.Y. Lee, T. Chung, Y.H. Moon, Arabidopsis Qc-SNARE gene AtSFT12 is involved in salt and osmotic stress responses and Na^+ accumulation in vacuoles, Plant Cell Rep. 34 (2015) 1127–1138.
[64] D. Singh, N.S. Yadav, V. Tiwari, P.K. Agarwal, B. Jha, A SNARE-like superfamily protein SbSLSP from the halophyte salicornia brachiata confers salt and drought tolerance by maintaining membrane stability K(+)/Na(+) ratio, and antioxidant machinery, Front. Plant Sci. 7 (2016) 737.
[65] X. Peng, X. Ding, T. Chang, Z. Wang, R. Liu, X. Zeng, Y. Cai, Y. Zhu, Overexpression of a vesicle trafficking gene OsRab7, enhances salt tolerance in rice, Sci. World J. 2014 (2014) 1–7.
[66] Y. Leshem, L. Seri, A. Levine, Induction of phosphatidylinositol 3-kinase-mediated endocytosis by salt stress leads to intracellular production of reactive oxygen species and salt tolerance, Plant J. 51 (2007) 185–197.
[67] X. Li, X. Wang, Y. Yang, R. Li, Q. He, X. Fang, D.-T. Luu, C. Maurel, J. Lin, Single-molecule analysis of PIP2;1 dynamics and partitioning reveals multiple modes of Arabidopsis plasma membrane aquaporin regulation, Plant Cell 23 (2011) 3780–3797.
[68] D.-T. Luu, A. Martinière, M. Sorieul, J. Runions, C. Maurel, Fluorescence recovery after photobleaching reveals high cycling dynamics of plasma membrane aquaporins in Arabidopsis roots under salt stress, Plant J. 69 (2012) 894–905.
[69] M. Reguera, E. Bassil, E. Blumwald, Intracellular NHX-type cation/H+ antiporters in plants, Mol. Plant 7 (2014) 261–263.